



HHS Public Access

Author manuscript

Eur J Neurosci. Author manuscript; available in PMC 2017 January 01.

Published in final edited form as:

Eur J Neurosci. 2016 January ; 43(2): 245–257. doi:10.1111/ejn.13124.

Alteration of SLP2-like Immunolabeling in Mitochondria Signifies Early Cellular Damage in Developing and Adult Mouse Brain

Yury M. Morozov¹, Yu-Yo Sun², Chia-Yi Kuan², and Pasko Rakic¹

¹Department of Neurobiology, Yale University School of Medicine and Kavli Institute for Neuroscience, 06510 New Haven, CT, USA

²Department of Pediatrics, Emory University School of Medicine and Children's Healthcare of Atlanta, Atlanta, Georgia, United States of America

Abstract

Mitochondria play a critical role in various pathways of regulated cell death. Here we propose a novel method for detection of initial derangement of mitochondria in degenerating and dying neuronal cells. The method is based on our recent finding that antibodies directed against the cannabinoid type 1 receptor (CB₁) also bind the mitochondrial stomatin-like protein 2 (SLP2) that belongs to an inner mitochondrial membrane protein complex. It is well established that SLP2 regulates mitochondrial biogenesis and respiratory functions. We now show that anti-CB₁ antibodies recognize conformational epitopes, but not linear amino acid sequence of SLP2. In addition we found that anti-CB₁ serum mostly labels swollen mitochondria with early or advanced stages of pathology in mouse brain while other proteins of the complex may mask epitopes of SLP2 in the normal mitochondria. Although neurons and endothelial cells in healthy brains contain occasional immunopositive mitochondria detectable with anti-CB₁ serum, their numbers increase significantly after hypoxic insults in parallel with signs of cellular damage. Moreover, use of electron microscopy suggests relocation of SLP2 from its normal functional position in the inner mitochondrial membrane into the mitochondrial matrix in pathological cells. Thus, SLP2-like immunolabeling serves as an *in situ* histochemical target detecting early derangement of mitochondria. Anti-CB₁ serum is crucial for this purpose because available anti-SLP2 antibodies do not provide selective labeling of mitochondria in the fixed tissue. This new detection method of mitochondrial dysfunction can benefit the *in vitro* research of human diseases and developmental disorders by enabling analysis in live animal models.

Keywords

mitochondrial permeability transition; MPTP complex; biomarker; antibody cross-reactivity; CB₁; SLP2

Introduction

Mitochondria are extremely dynamic multifunctional organelles that play important roles in the triad of regulated cell death – apoptosis, necrosis and autophagic cell death - pathways. Mitochondrial fragmentation versus biogenesis is also a critical step in the initiation of neurodegeneration (Chan, 2006; Lin & Beal, 2006; Knott *et al.*, 2008; Green *et al.*, 2011). The theme emerged from past research is that many mitochondrial proteins need to be properly positioned to execute physiological functions, while their mis-location triggers cellular injury. For example, during mitochondrial membrane permeabilization, cytochrome c and other toxic proteins are leaked into the cytosol to trigger caspase-mediated apoptosis (Galluzzi *et al.*, 2009). Whether mitochondrial intermembrane space proteins are relocated into the mitochondrial matrix during regulated cell death, however, is unclear although several mechanisms of intra-mitochondrial protein relocation during normal mitochondrial function are known (e.g., Neupert & Herrmann, 2007).

Stomatin-like protein 2 (SLP2) is a constitutive mitochondrial protein that is attached to the inner mitochondrial membrane (IMM) through protein complexes (Da Cruz *et al.*, 2003; 2008). SLP2 regulates at least two important aspects of mitochondrial functions. First, SLP2 recruits prohibitins to cardiolipin-enriched microdomains in which electron transport complexes are optimally assembled (Da Cruz *et al.*, 2008; Christie *et al.*, 2011). Second, SLP2 interacts with mitofusin 2 and is required for stress-induced mitochondrial hyperfusion (Hajek *et al.*, 2007; Tondera *et al.*, 2009). In cultured SLP2-deficient immune cells, the mitochondrial respiratory functions are reduced (Christie *et al.*, 2012; Mitsopoulos *et al.*, 2015). Yet little is known of how SLP2 responds to mitochondrial dysfunction during early steps of regulated cell death.

Recently, we demonstrated that made-in-Guinea pig polyclonal serum directed to the last 31 amino acids (L31) of cannabinoid type 1 receptor (CB₁) also binds SLP2 in a subset of mitochondria in addition to its normal targets of CB₁-expressing neurons. This cross-reactivity is specific, as shown by mass spectrometry identification of anti-CB₁ immunoprecipitates and immunoblotting response to transfected SLP2 cDNA (Morozov *et al.*, 2013). Although our published and novel data do not necessarily disprove recently suggested mitochondrial CB₁ (Benard *et al.*, 2012; Hebert-Chatelain *et al.* 2014; Morozov *et al.*, 2014), similar immunolabeling in wild type and CB₁-null mice indicates, at least parallel, non-CB₁ labeling in the mitochondria (present research). Our data together with a recent demonstration of a non-CB₁ mechanism of the CB₁ ligands action to the respiratory activity of isolated mitochondria (Fisar *et al.*, 2014; Singh *et al.*, 2015) warrant further investigation of the problem. In the present study, we show that the anti-CB₁ antibody preferentially labels presumable SLP2 misplaced in the matrix of disordered mitochondria, and that the number of immunopositive mitochondria detectable with anti-CB₁ serum increases in parallel with postmortem hypoxia in the embryos and after hypoxic-ischemic insults in adult mouse brains. These results suggest that misplaced SLP2 is a novel histochemical marker of mitochondrial dysfunction and early cellular injury that occurs sporadically in healthy, and ubiquitously in hypoxia-exposed developing and adult mouse brains.

Materials and Methods

All animal protocols were approved by the Institutional Animal Care and Use Committee of Yale University and Emory University and comply with the National Institutes of Health (USA) guidelines for animal care and use. For terminal surgery, the animals were deeply anaesthetized with sodium pentobarbital (3 ml/kg body weight) or euthasol (0.5 ml/kg body weight).

Western blot analysis of mitochondrial fractions

CD-1 mouse embryos at E13.5 (n=4), E16.5 (n=6) or new-born mice (n=6) were decapitated and forebrains were removed. Crudely purified mitochondrial fractions were prepared as described (Morozov *et al.*, 2013). 20 µg protein samples were separated using electrophoresis at 210V in 4-12% NuPAGE Bis-Tris mini gels (Invitrogen, Carlsbad, CA, USA) and electrophoretically transferred to PVDF membranes (Bio-Rad Laboratories, Hercules, CA, USA). The membranes were subsequently immunoblotted with anti-CB₁-L31 (made-in-Guinea pig; Frontier Science Co. Ltd, Japan; 1:400) and anti-SLP2 (made-in-rabbit; 1:200; Santa Cruz Biotechnology Inc, Santa Cruz, CA, USA). The membranes were counterstained using corresponding donkey anti-Guinea pig (1:5000; Jackson Immunoresearch, West Grove, PA, USA) or goat anti-rabbit (1:3000; Bio-Rad Laboratories, Hercules, CA, USA) horse radish peroxidase conjugates, immersed in Clarity Western ECL Substrate (Bio-Rad Laboratories, Hercules, CA, USA) and exposed to X-ray films during recorded periods. Between the immunoblot procedures, membranes were rinsed and incubated in Restore Western Blot Stripping Buffer (Thermo Scientific; Rockford, IL, USA). Before repetitive immunoblots, the membranes were kept in Tris-saline buffer (pH 7.5) at +4°C for 4 days.

Immunocytochemistry for light and electron microscopy

CD-1 mouse embryos of the following ages were used: E12.5 (n=4), E13.5 (n=32), E16.5 (n=10) and E17.5 (n=9). E13.5 CB₁-null embryos (n=4) and heterozygote littermates (n=3) in C57BL6 background genotyped as previously described were also used (generation was sponsored by NIMH, Bethesda, MD, USA; Zimmer *et al.*, 1999). The embryos were decapitated and the embryo brains were removed and immersed overnight in a fixative containing 4% paraformaldehyde, 0.2% picric acid and 0.2% glutaraldehyde. Coronal 100-µm-thick brain sections were cut with a vibratome and used for immunocytochemistry.

Several polyclonal anti-CB₁ (C-terminus) antibodies against L31 of mouse CB₁ were used. Namely, one made-in-goat (catalog number CB1-Go-Af450; dilution 1:500) and two lots of made-in-Guinea pig (catalog numbers CB1-GP-Af530 and CB1-GP-Af530-1; 1:2000) all from Frontier Science Co. Ltd, Japan. We also used antibodies for the last 15 amino acids (L15, C-terminus; 1:1000) and amino-terminus (NH; 1:1000) of rat CB₁ (both made-in-rabbit; gifts from K. Mackie, Indiana University, IN, USA). Corresponding biotinylated anti-guinea pig, anti-goat or anti-rabbit IgGs (1:300) and the Elite ABC kit (all from Vector Laboratories, Burlingame, CA, USA) with Ni-intensified 3,3'-diaminobenzidine-4HCl (DAB-Ni) as a chromogen were applied. For the immunogold/silver procedure, anti-CB₁-L31 made-in-Guinea pig primary antibodies (1:200) and made-in-goat anti-Guinea pig

secondary serum conjugated with 1-nm gold particles (1:80; Aurion, Wageningen, The Netherlands) were used. Silver-intensification of gold was performed with Aurion R-Gent SE-LM according to the manufacturer's instructions. Thereafter, sections were post-fixed with OsO₄, dehydrated, and then embedded in durcupan ACM (Fluka, Buchs, Switzerland) on microscope slides and coverslipped. Selected fragments of tissue were analyzed and photographed with an Axioplan 2 microscope (Zeiss, Jena, Germany) and re-embedded into durcupan blocks for electron microscopic investigation. The samples were cut with a Reichert ultramicrotome into 70-nm-thick sections. The sections were then stained with lead citrate and evaluated and photographed in a JEM 1010 electron microscope (JEOL, Japan) equipped with a Multiscan 792 digital camera (Gatan, Pleasanton, CA, USA). The specificity of the method and antibodies were confirmed by replacing primary antibodies with normal Guinea pig serum (1:500 for DAB-Ni staining or 1:100 for gold/silver procedure; Jackson Immunoresearch, West Grove, PA, USA) or pre-absorption of anti-CB₁ serum with the antigen peptide (20 µg/ml; Frontier Science Co. Ltd, Japan). No mitochondrial staining was observed in these specimens either by light or electron microscopy.

Three-dimensional (3D) reconstruction from electron micrographs and morphometry of the mitochondria

Serial micrographs (made from every section of a 30-60-section series) of selected cells were obtained with 12,000-20,000× magnification of the microscope as previously described (Morozov *et al.*, 2006). 3D reconstruction and measurements of volume of the reconstructed mitochondria were performed using Reconstruct software (Fiala, 2005), publicly available at <http://synapses.bu.edu>. The estimated length of reconstructed mitochondria was calculated as the hypotenuse of a triangle with one catet measured as the maximal horizontal shift of the profiles in the serial sections and the other catet as the number of sections in which the mitochondrial profiles are seen multiplied by the thickness of the sections. The estimated length of branched mitochondria was calculated as the sum of the lengths of their simple fragments. Truncated mitochondria were treated “as is” in the quantification if their estimated length was more than the average length of the non-truncated mitochondria in the same group; if not, they were ignored. The mean diameter of the reconstructed mitochondria was calculated based upon the volume formula for ellipsoids using the lengths, as measured above, as the longest diameter of the ellipsoid.

Induction of anoxia in the embryonic brain

Dissected heads from mouse embryos (wild type, CB₁-null and heterozygote littermates; totally n=44 embryos) at E13.5 were placed in an incubator at +37°C in physiological solution in closed vials (anoxic conditions) or when constantly bubbled with 95% O₂ / 5% CO₂ (oxygenation). After 1, 3, 4.5 and 6 hours, the heads were immersed in fixative and prepared for immunocytochemistry analysis as above.

Quantification of immunopositive mitochondria

Quantification of immunopositive mitochondria in the mouse embryo brain sections was performed after above-described immunolabeling. Both hemispheres of two random coronal

sections made through the middle of the forebrain from E13.5 embryos were used for counting. Counting of mitochondria identified as immunopositive particles was performed in a BH-2 conventional microscope (Olympus, Japan), equipped with a 100× oil immersion objective and a 15× eyepiece with grid. By 5 fields (10×10 μm at 100× objective) from lateral ganglionic eminence (LGE), neocortex, dorsal arch and hippocampus were analyzed in every section while focusing through the total thickness of the section (100 μm). The fields from the VZ/SVZ were chosen for counting randomly, but blood vessels were avoided. Occasional CB₁-immunopositive axons were ignored.

Induction of hypoxia-ischemia in adult mouse brains

The induction of transient hypoxic-ischemic (tHI) brain injury in adult mice was performed as previously reported (Adhami *et al.*, 2006; Sun *et al.*, 2014). Briefly, male C57BL/6 mice at the age of 10 to 13 weeks were anesthetized under 2% isoflurane to perform transient occlusion of the right common carotid artery with two releasable knots of 4.0 silk suture, which were released after the hypoxic stress. To induce hypoxia, mice were infused with 7.5% O₂/92.5% N₂ through a face-mask for 30 min, while the animal core body temperature was maintained at 37.5 ± 0.5°C using a rectal thermoprobe coupled to a heating lamp. After designed periods of survival (0 min, 30 min, 1 hr, and 3 hr after tHI), animals were transcardially perfused with a fixative containing 4% paraformaldehyde and 0.5% glutaraldehyde. Coronal 60-μm-thick brain sections were cut with a vibratome and used for immunocytochemistry as above.

Quantification of immunopositive mitochondria-containing cells in adult mouse brain

Quantification of immunopositive mitochondria-containing cells was performed in tHI-exposed and normoxia control animals. Totally 15 mice were analyzed. A hippocampal neuron (regardless of its zone or laminar position) was counted as immunopositive if more than 10 labeled particles were seen in cytoplasm of the cell body. Singular immunopositive particles in the neuropil were ignored. Counting was performed in a BH-2 conventional microscope (Olympus, Japan), equipped with a 40× dry objective. By 3 coronal sections of rostral hippocampus from each animal were analyzed and then photographed with an Axioplan 2 microscope (Zeiss, Jena, Germany) equipped with a 5× objective and area of the hippocampus was measured with ImageJ software (NIH, Wayne Rasband, USA). Number of cells counted was normalized for 1 mm².

Statistical analysis

Statistical analysis was analyzed by unpaired *t*-test using Excel 2013 (Microsoft) software. A value of *P*<0.05 was considered significant. Values were expressed as mean ± SD in quantification of mitochondrial volume, length, diameter, length/diameter ratio and immunopositive mitochondria; and mean ± SEM in quantification of immunopositive mitochondria-containing cells.

Results

Anti-CB₁-L31 antibodies recognize conformational epitope of SLP2

Because SLP2 is widely expressed in mitochondria while anti-CB₁-L31 sera only labels a fraction of those in mouse brains, we hypothesize that these antibodies recognize conformational epitopes of SLP2 that are unmasked in specific physiological or pathological conditions. To test this possibility, we used the phenomenon of spontaneous protein refolding after denaturing electrophoresis to compare the properties of anti-CB₁-L31 and anti-SLP2 antibodies (Chan *et al.*, 2008).

Western blot membrane containing electrophoresis-separated proteins from mitochondrial fractions was re-probed 4 times during a seven-day period. Soon after electrophoresis, anti-CB₁-L31 serum (made-in-Guinea pig) produced weak, if any, labeling; whereas anti-SLP2 serum perfectly labeled SLP2 molecules (Fig. 1). Re-probing the same blot 5 days later with same anti-CB₁-L31 serum showed intensified immunolabeling, whereas re-probing with the anti-SLP2 antibody led to marked reduction of signals (Fig. 1). These results suggest that anti-SLP2 antibody recognizes linear peptide epitope(s) that predominate at denaturing electrophoresis conditions; whereas anti-CB₁-L31 antibody reacts to conformational epitopes in CB₁ and SLP2 that were recovered after refolding of the proteins. Anti-CB₁-L31 immunoblot reveals both, ~40 kDa and ~35 kDa, forms of SLP2, suggesting that the epitope of anti-CB₁-L31 antibodies is common for both light and heavy forms of SLP2 (see the Basic Local Alignment Search Tool at <http://www.ncbi.nlm.nih.gov/blast/Blast.cgi>).

Two types of immunopositive mitochondria in the embryonic mouse brain have distinct identity

Binding of the anti-CB₁-L31 sera with supposed SLP2 identifies two patterns of immunopositive mitochondria that probably execute distinct functions. Both these patterns are rare in the normal embryonic brain (generally less than 1% of all mitochondria); but, those frequency depends of the cellular and tissue physiological conditions (see below). One population, previously designated as “type 1” (Morozov *et al.*, 2013), exhibits the antigen in the mitochondrial intermembrane space corresponding to the normal location of SLP2 (Fig. 2A, B; Da Cruz *et al.*, 2003). The other population, designated as “type 2”, demonstrates immunoprecipitation in the mitochondrial matrix (Fig. 2C-F) that is an unusual location for SLP2 in functional mitochondria (Da Cruz *et al.*, 2008) and, as we hypothesis, results from its intramitochondrial relocation.

Three-dimensional (3D) reconstruction and morphometric analysis of mitochondria show that type 1 immunopositive mitochondria, on average, have the same length and diameter as immunonegative mitochondria (Table 1). In contrast, the type 2 mitochondria demonstrate a variety of ultrastructural pathologies from slightly increased diameter to noticeable swelling and lysis of the inner compartment (see micrographs and morphometric data below). In a normal developing mouse brain, type 2 mitochondria concentrate in sporadically distributed cells such as immature projection neurons (Fig. 2C), endothelial cells lining blood capillary walls (Fig. 2D) and mitotic cells in the ventricular zone (presumed neuronal stem cells; Fig. 2E, F).

In the present study, we focus on the link of type 2 mitochondria (hereafter referred to as “immunopositive” mitochondria) to apparent cellular damage, while the causes for the rare type 1 mitochondria are reserved for future investigation.

Immunopositive mitochondria expose ultrastructural pathology of distinct cells in developing brain

In the normal developing mouse brain, we detected sporadic spots of neuropil containing numerous immunopositive mitochondria while surrounding tissue was immunonegative (Fig. 3A, B). Electron microscopy study reveals that some of the immunopositive mitochondria-containing cells demonstrate minor ultrastructural pathology, namely, enlarged nuclear membranes and/or slightly swollen mitochondria (Fig. 3C, D). Other cells, however, show severe ultrastructural pathology, including considerable swelling of all mitochondria, the nuclear membrane, and cisterns of the rough endoplasmic reticulum, leading to near-complete degradation of cytoplasm (Fig. 3E-H). Regardless of the degree of damage of the immunopositive mitochondria-containing cells, adjacent cells containing only immunonegative mitochondria demonstrate an ultrastructure characteristic of normal developing neurons. These observations correspond with reported local spontaneous deviations from normal neuronal development (Torii *et al.*, 2009).

Our correlated light-electron microscopy analysis of capillaries in the embryo brain also shows that immunopositive mitochondria in distinct endothelial cells are associated with different degree of ultrastructural pathology. Namely, some of the immunopositive mitochondria-containing endothelial cells demonstrate minor ultrastructural pathology such as swollen cisterns of the rough endoplasmic reticulum, while most of other organelles remain unchanged. Other immunopositive mitochondria-containing capillaries show major ultrastructural pathology, including swelling and degradation of all the mitochondria. Immunonegative segments of blood vessels demonstrate normal ultrastructure even if they situate near damaged ones that contain immunopositive mitochondria (Fig. 4).

Morphometric characterizations of 3D-reconstructed mitochondria in developing projection neurons and endothelial cells show that the length of mitochondria gradually decreases and their diameter increases as the cell ultrastructural pathology becomes more apparent. Finally, immunopositive mitochondria-containing cells demonstrating major ultrastructural pathologies retain swollen sphere-shaped mitochondria (Fig. 5; Table 1).

The link to similar cellular pathology by immunopositive mitochondria in different cell types such as neurons and endothelial cells (together with our unfinished study of liver cells and adipocytes) suggest that translocation of SLP2 from the intermembrane space to the matrix may be a common phenomenon during early cellular damage.

Anoxia up-regulates immunopositive mitochondria in the embryo brain

The ultrastructural pathology of the immunopositive mitochondria-containing cells (swollen organelles and lightened cytoplasm) resembles those for necrosis and hypoxic-ischemic injury (Bredesen *et al.*, 2006; Adhami *et al.*, 2006). To test this mechanistic link, we compared anti-CB₁-L31 (made-in-Guinea pig) staining of postmortem E13.5 mouse brains

in dissected heads that were immersed in +37°C saline solution in anoxic conditions or bubbled with oxygen. In anoxic conditions, a marked increase of immunopositive mitochondria in all brain segments was noticed after 4.5-6 hr incubation, whereas this number was reduced by oxygenation (Fig. 6A; Table 2). The low number of immunopositive mitochondria and normal cellular ultrastructure in less than 3 hr anoxia may reflect a higher resistance to hypoxia by mammalian embryos (Martin et al., 2010; Ikonomidou & Kaindl, 2011). The marked increase of immunopositive mitochondria in the neuropil at 4.5 and 6 hr anoxic incubation was paralleled with necrotic-like cellular ultrastructural pathology demonstrating strict dependence of mitochondrial labeling from physiological conditions of the tissue and cells (Fig. 6B-G).

Comparing different sera and protocols for detection of disordered mitochondria

Our finding that anoxia imperatively and dramatically up-regulates mitochondria immunopositive for the made-in-Guinea pig anti-CB₁-L31 serum provides an opportunity to perform accurate control experiments as well as to investigate efficiency of other sera and immunolabeling protocols for detection of disordered mitochondria. First of all, we discovered numerous immunopositive mitochondria in the CB₁-null embryos after 4.5 hr of anoxia. Matrix location of the antigen in the CB₁-null embryos identical to wild type ones (e.g., Figures 2-4, 6) was confirmed with electron microscopy (Fig. 7A-C) while quantification with light microscopy shows a nearly equal number of immunopositive mitochondria in CB₁-null and wild type embryos (Fig. 7L). This further validates presence of a non-CB₁ antigen in the mitochondrial labeling at least in this experimental paradigm. Conversely, pre-absorption of the anti-CB₁-L31 serum with the antigen peptide (L31) or replacement of the primary antibodies with the normal serum abolishes the mitochondrial immunolabeling in CB₁-null and wild type littermates (Fig. 7B, J). This confirms specificity of the staining and rules out the possibility that the observed DAB-Ni precipitation results from unequal specimen preparations or mitochondrial endogenous biotin, peroxidase or reactive oxygen species reported for other experimental models (e.g., Hollinshead *et al.*, 1997; Belikova *et al.*, 2006; Lorincz & Nusser, 2008).

As an additional control, we performed immuno-gold/silver labeling with made-in-Guinea pig anti-CB₁-L31 as the primary serum confirming location of the antigen in the mitochondrial matrix whereas staining in the intermembrane space was not encountered (Fig. 7C, D). Counting of well-identified selective (canonical CB₁ and mitochondrial) versus presumed background (cytoplasmic, nuclear or extracellular) labeling in the anoxia-exposed embryos obtained with different chromogens (see Materials and Methods for experimental conditions) shows that among immuno-gold/silver particles seen in the electron microscope only about 20% are specific whereas immuno-peroxidase DAB-Ni staining provides higher specificity – about 90%.

We also found that sera raised to other segments of CB₁ (L15 and NH-terminus) do not provide robust mitochondrial labeling in postmortem embryos that could be detectable in light or electron microscopy (Fig. 7H, I, L). Surprisingly made-in-goat serum raised to L31 produces sporadic dotted staining (arrowheads) that looks similar to mitochondrial labeling in light microscopy but are less numerous (Fig. 7J, L). Nevertheless comprehensive study in

the electron microscope demonstrated that such dotted staining represents cytoplasmic labeling of an unknown phenotype whereas immunopositive mitochondria were not encountered in these specimens (Fig. 7K). This indicates that although the made-in-goat and made-in-Guinea pig sera were raised to the same L31 peptide they actually recognize different epitopes (at least in mitochondria) which require further investigation. Our observations identify anti-CB₁-L31 made-in-Guinea pig serum as a novel instrument for *in situ* visualization of disordered mitochondria. Other antibodies that effectively label disordered mitochondria are not known for us.

tHI up-regulates immunopositive mitochondria in the adult mouse brain

Finally, we applied anti-CB₁-L31 (made-in-Guinea pig) serum with immuno-peroxidase DAB-Ni staining for investigation of the ultrastructural pathological responses to transient hypoxia-ischemia (tHI) insult in adult mouse brains, which simulates thrombotic stroke (Adhami *et al.*, 2006; Sun *et al.*, 2014). We focused quantitative analysis of the immunopositive mitochondria for the hippocampus, although similar changes were found in other tHI-affected brain regions. Our analysis showed that tHI does not modify the canonical CB₁ immunolabeling in cell bodies and axons of the cholecystinin-expressing interneurons (Katona *et al.*, 1999; Morozov & Freund, 2003). In contrast, numerous immunopositive mitochondria were detected in the tHI-exposed hemisphere, and a smaller amount in the contralateral side (Fig. 8). In tHI-exposed adult mice, similar to the responses in postmortem embryo brains (Fig. 6), the emergence of immunopositive mitochondria was associated with ultrastructural pathology, such as mitochondrial swelling. In the contralateral side, the majority of mitochondria has tubular shape with diameter 250-300 nm, characteristic for healthy neurons. Quantification shows increase of neurons containing numerous immunopositive mitochondria during the first hour following tHI (Fig. 8G). Its subsequent decrease in 3 hr after tHI coincides with massive death of cells that presumably destroys mitochondrial proteins including the supposed SLP2 epitope (research in progress). Thus, immunolabeling of mitochondria with anti-CB₁-L31 (made-in-Guinea pig) serum reveals dynamics of mitochondrial disorganization in different tissues and sheds new light on the mechanisms of hypoxia-ischemia-induced brain damage.

Discussion

Owing to its critical role during regulated cell death and cellular physiology, the mitochondria have been heavily studied leading to many immunological and biochemical methods to assess their functions and dysregulation. Yet, the majority of current methods is applicable only to cultured cells or requires organelle fractionation. To date, there are no *in situ* histochemical methods to detect disordered mitochondria in live animals. The presented results help to fill this void and shed new insights into ultrastructural alterations of degenerating mitochondria.

We show that made-in-Guinea pig antibodies directed against L31 of CB₁ additionally recognize SLP2, a mitochondrial inner membrane-associated protein that faces the intermembrane space in its functional position and maintains mitochondrial stability (Da Cruz *et al.*, 2008; Christie *et al.*, 2012; Mitsopoulos *et al.*, 2015). Double specificity of the

made-in-Guinea pig CB₁-L31 antibodies was unequivocally demonstrated in our mass spectrometry identification of anti-CB₁ immunoprecipitates and immunoblotting of cultured neuroblastoma cells transfected with SLP2 cDNA (Morozov *et al.*, 2013). Anti-CB₁ sera are crucial for histochemical detection of SLP2 because available anti-SLP2 antibodies are applicable only in Western blots whereas they produce background staining of cytoplasm rather than selective labeling of mitochondria in the fixed tissue (our data not shown). Further, the epitopes of SLP2 recognized by anti-CB₁-L31 antibodies are conformational; i.e., the antibodies recognize the peptide folded in secondary structure, but not its denatured form. Presumably, the assembly of SLP2 with mitofusin 2 and other proteins into a complex on the inner mitochondrial membrane blocks the immunolabeling, whereas dissociation of the complex likely releases SLP2 for binding with anti-CB₁-L31 antibodies in the type 1 mitochondria (Hajek *et al.*, 2007; Da Cruz *et al.*, 2008; Christie *et al.*, 2011; Mitsopoulos *et al.*, 2015; Fig. 9). Moreover, we hypothesize that severe hypoxic insult stimulates relocation of SLP2 into the mitochondrial matrix where it becomes accessible to the anti-CB₁-L31 antibodies. This scenario could account for why anti-CB₁-L31 serum preferentially binds SLP2 in disordered (type 2) mitochondria, which are up-regulated in anoxic conditions and linked to cellular ultrastructural pathology. The alternative scenario of up-regulated immunopositive mitochondria due to de novo biosynthesis of SLP2 is less likely, because swollen mitochondria can hardly provide ATP energy for protein synthesis (Ahmad *et al.*, 2013). As mitochondrial degeneration proceeds, the epitope of SLP2 is probably gradually lost due to severe denaturation or degradation of mitochondrial proteins including SLP2 (Fig. 9). The last scenario could explain why the massive emergence of immunopositive mitochondria in tHI-exposed brain is temporal and a subset of severely disordered mitochondria does not exhibit immunolabeling in our electron microscopy observations.

Our observations further suggest that removal of SLP2 from IMM, if occurs, may contribute or follow to mitochondrial dysfunction such as opening of the mitochondrial permeability transition pore that leads to dissipation of the mitochondrial transmembrane potential (Ψ_m) and arrest of mitochondrial ATP synthesis; osmotic breakdown of the outer mitochondrial membrane and release of the intermembrane space proteins (e.g., cytochrome C and apoptosis-inducing factor) into the cytosol, where they promote cell death (Chan, 2006; Lin & Beal, 2006; Kroemer *et al.*, 2007; Knott *et al.*, 2008; Green, *et al.*, 2011; Galluzzi *et al.*, 2009; Vanlangenakker *et al.*, 2012). Several lines of evidence support this hypothesis: first, the role of SLP2 in maintaining mitochondrial stability has been reported (Da Cruz *et al.*, 2008; Mitsopoulos *et al.*, 2015); second, observed here osmotic swelling of the mitochondrial matrix resembles morphological correlates of necrosis secondary to IMM permeabilization (e.g., Galluzzi *et al.*, 2009; Green *et al.*, 2011); and third, hypoxia-induced up-regulation of immunopositive mitochondria (present research) reproduces known link between oxidative stress and mitochondrial dysfunction (e.g., Lin & Beal, 2006).

Our unexpected finding also raises many questions for further investigation. For example, what is the 3D structure of the SLP2 epitope that is recognized by anti-CB₁-L31 antibodies; if this occurs, what is the mechanism by which SLP2 is detached from IMM; are the minor morphofunctional deviations of mitochondria associated with immunolabeling reversible?

Regardless of the prospective answers, the observed mitochondrial phenotype provides a new target for early diagnosis of cell degeneration in postnatal and developing central nervous and vascular systems. The suggested approach identifies early mitochondrial dysfunction complementing popular immunohistochemical detection of cytoplasmic reactions (e.g., active caspases) that may reveal descending pathways of the programmed cell death. This novel method can detect deviations in mitochondrial functionality not only *in vitro*, but also *in situ* in complex tissues such as the mammalian brain, partially covering the gap in contemporary methodical arsenal.

Acknowledgments

The authors declare no competing financial interests. We are grateful to Ruth Rappaport, Ph.D. for her editorial assistance in preparation of the manuscript. Y.M.M. initiated the project, performed experiments and wrote the article; Y.Y.S. performed tHI; C.-Y. K. and P.R. analyzed the data and wrote the article. This research was supported by Kavli Institute for Neuroscience at Yale and the National Institute of Health grants DA023999, NS014841 and R01EY002593 (to P.R.) and NS084744 (to C.-Y.K.).

References

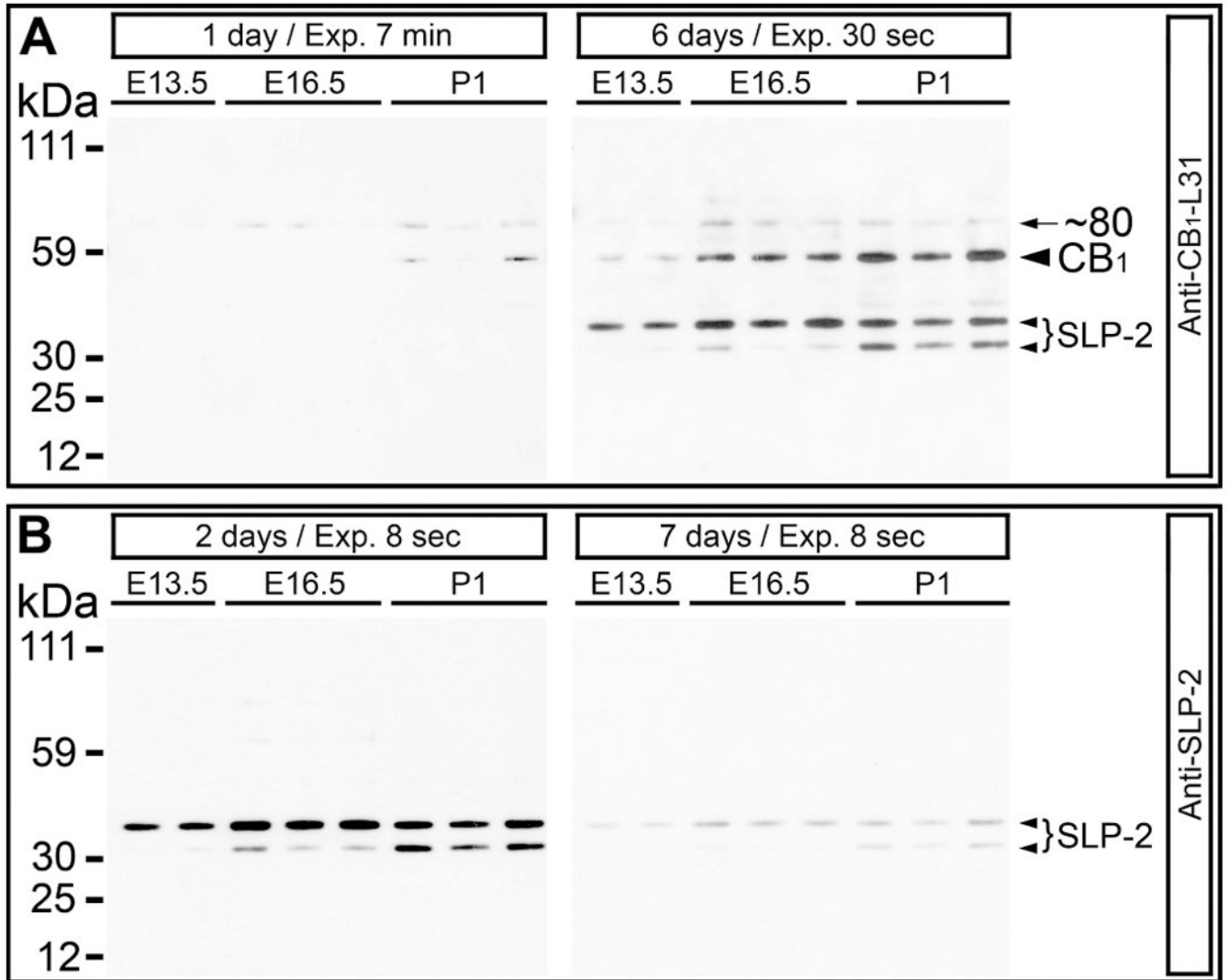
- Adhami F, Liao G, Morozov YM, Schloemer A, Schmithorst VJ, Lorenz JN, Dunn RS, Vorhees CV, Wills-Karp M, Degen JL, Davis RJ, Mizushima N, Rakic P, Dardzinski BJ, Holland SK, Sharp FR, Kuan CY. Cerebral Ischemia-Hypoxia Induces Intravascular Coagulation and Autophagy. *Am J Pathol.* 2006; 169:566–583. [PubMed: 16877357]
- Ahmad T, Aggarwal K, Pattnaik B, Mukherjee S, Sethi T, Tiwari BK, Kumar M, Micheal A, Mabalirajan U, Ghosh B, Sinha Roy S, Agrawal A. Computational classification of mitochondrial shapes reflects stress and redox state. *Cell Death Dis.* 2013; 4:e461. [PubMed: 23328668]
- Belikova NA, Vladimirov YA, Osipov AN, Kapralov AA, Tyurin VA, Potapovich MV, Basova LV, Peterson J, Kurnikov IV, Kagan VE. Peroxidase activity and structural transitions of cytochrome *c* bound to cardiolipin-containing membranes. *Biochemistry.* 2006; 45:4998–5009. [PubMed: 16605268]
- Benard G, Massa F, Puente N, Lourenço J, Bellocchio L, Soria-Gómez E, Matias I, Delamarre A, Metna-Laurent M, Cannich A, Hebert-Chatelain E, Mülle C, Ortega-Gutiérrez S, Martín-Fontecha M, Klugmann M, Guggenhuber S, Lutz B, Gertsch J, Chaouloff F, López-Rodríguez ML, Grandes P, Rossignol R, Marsicano G. Mitochondrial CB₁ receptors regulate neuronal energy metabolism. *Nat Neurosci.* 2012; 15:558–564. [PubMed: 22388959]
- Bredesen DE, Rao RV, Mehlen P. Cell death in the nervous system. *Nature.* 2006; 443:796–802. [PubMed: 17051206]
- Chan CS, Winstone TM, Turner RJ. Investigating protein-protein interactions by far-Westerns. *Adv Biochem Eng Biotechnol.* 2008; 110:195–214. [PubMed: 18219468]
- Chan DC. Mitochondria: dynamic organelles in disease, aging and development. *Cell.* 2006; 125:1241–1252. [PubMed: 16814712]
- Christie DA, Lemke CD, Elias IM, Chau LA, Kirchhof MG, Li B, Ball EH, Dunn SD, Hatch GM, Madrenas J. Stomatin-like protein 2 binds cardiolipin and regulates mitochondrial biogenesis and function. *Mol Cell Biol.* 2011; 31:3845–3856. [PubMed: 21746876]
- Christie DA, Mitsopoulos P, Blagih J, Dunn SD, St-Pierre J, Jones RG, Hatch GM, Madrenas J. Stomatin-like protein 2 deficiency in T cells is associated with altered mitochondrial respiration and defective CD4⁺ T cell responses. *J Immunol.* 2012; 189:4349–4360. [PubMed: 23028053]
- Da Cruz S, Parone PA, Gonzalo P, Bienvenut WV, Tondera D, Jourdain A, Quadroni M, Martinou JC. SLP2 interacts with prohibitins in the mitochondrial inner membrane and contributes to their stability. *Biochim Biophys Acta.* 2008; 1783:904–911. [PubMed: 18339324]
- Da Cruz S, Xenarios I, Langridge J, Vilbois F, Parone PA, Martinou JC. Proteomic analysis of the mouse liver mitochondrial inner membrane. *J Biol Chem.* 2003; 278:41566–41571. [PubMed: 12865426]

- Fiala JC. Reconstruct: a free editor for serial section microscopy. *J Microsc.* 2005; 218:52–61. [PubMed: 15817063]
- Fišar Z, Singh N, Hroudová J. Cannabinoid-induced changes in respiration of brain mitochondria. *Toxicol Lett.* 2014; 231:62–71. [PubMed: 25195527]
- Galluzzi L, Blomgren K, Kroemer G. Mitochondrial membrane permeabilization in neuronal injury. *Nat Rev Neurosci.* 2009; 10:481–494. [PubMed: 19543220]
- Green RD, Galluzzi L, Kroemer G. Mitochondria and the autophagy-inflammation-cell death axis in organismal aging. *Science.* 2011; 333:1109–1112. [PubMed: 21868666]
- Hajek P, Chomyn A, Attardi G. Identification of a novel mitochondrial complex containing Mitofusin 2 and Stomatin-like protein 2. *J Biol Chem.* 2007; 282:5670–5681. [PubMed: 17121834]
- Hebert-Chatelain E, Reguero L, Puente N, Lutz B, Chaouloff F, Rossignol R, Piazza PV, Benard G, Grandes P, Marsicano G. Cannabinoid control of brain bioenergetics: Exploring the subcellular localization of the CB1 receptor. *Mol Metab.* 2014; 3:495–504. [PubMed: 24944910]
- Hollinshead M, Sanderson &, Vaux DJ. Anti-biotin Antibodies Offer Superior Organelle-specific Labeling of Mitochondria over Avidin or Streptavidin. *J Histochem Cytochem.* 1997; 45:1053–1057. [PubMed: 9267466]
- Ikonomidou C, Kaindl AM. Neuronal death and oxidative stress in the developing brain. *Antioxid Redox Signal.* 2011; 14:1535–15350. [PubMed: 20919934]
- Katona I, Sperlagh B, Sik A, Kafalvi A, Vizi ES, Mackie K, Freund TF. Presynaptically located CB1 cannabinoid receptors regulate GABA release from axon terminals of specific hippocampal interneurons. *J Neurosci.* 1999; 19:4544–4558. [PubMed: 10341254]
- Knott AB, Perkins G, Schwarzenbacher R, Wetzel EB. Mitochondrial fragmentation in neurodegeneration. *Nat Rev Neurosci.* 2008; 9:505–518. [PubMed: 18568013]
- Kroemer G, Galluzzi L, Brenner C. Mitochondrial membrane permeabilization in cell death. *Physiol Rev.* 2007; 87:99–163. [PubMed: 17237344]
- Lin MT, Beal MF. Mitochondrial dysfunction and oxidative stress in neurodegenerative diseases. *Nature.* 2006; 443:787–795. [PubMed: 17051205]
- Lorincz A, Nusser Z. Specificity of immunoreactions: the importance of testing specificity in each method. *J Neurosci.* 2008; 28:9083–9086. [PubMed: 18784286]
- Martin DS, Khosravi M, Grocott MP, Mythen MG. Concepts in hypoxia reborn. *Crit Care.* 2010; 14:315. [PubMed: 20727228]
- Mitsopoulos P, Chang YH, Wai T, König T, Dunn SD, Langer T, Madrenas J. Stomatin-like Protein-2 is Required for In vivo Mitochondrial Respiratory Chain Supercomplex Formation and Optimal Cell Function. *Mol Cell Biol.* 2015; 35:1838–1847. [PubMed: 25776552]
- Morozov YM, Ayoub AE, Rakic P. Translocation of synaptically connected interneurons across the dentate gyrus of the early postnatal rat hippocampus. *J Neurosci.* 2006; 26:5017–5027. [PubMed: 16687493]
- Morozov YM, Dominguez MH, Varela L, Shanabrough M, Koch M, Horvath TL, Rakic P. Antibodies to cannabinoid type 1 receptor co-react with stomatin-like protein 2 in mouse brain mitochondria. *Eur J Neurosci.* 2013; 38:2341–2348. [PubMed: 23617247]
- Morozov YM, Freund TF. Post-natal development of type 1 cannabinoid receptor immunoreactivity in the rat hippocampus. *Eur J Neurosci.* 2003; 18:1213–1222. [PubMed: 12956720]
- Morozov YM, Horvath TL, Rakic P. A tale of two methods: Identifying neuronal CB1 receptors. *Mol Metab.* 2014; 3:338. [PubMed: 24944888]
- Morozov YM, Torii M, Rakic P. Origin, Early Commitment, Migratory Routes, and Destination of Cannabinoid Type 1 Receptor-Containing Interneurons. *Cerebral Cortex.* 2009; 19:i78–89. [PubMed: 19346272]
- Neupert W, Herrmann JM. Translocation of proteins into mitochondria. *Annu Rev Biochem.* 2007; 76:723–749. [PubMed: 17263664]
- Singh N, Hroudová J, Fišar Z. Cannabinoid-Induced Changes in the Activity of Electron Transport Chain Complexes of Brain Mitochondria. *J Mol Neurosci.* 2015; 56:926–931. [PubMed: 25820672]

- Sun YY, Morozov YM, Yang D, Li Y, Dunn RS, Rakic P, Chan PH, Abe K, Lindquist DM, Kuan CY. Synergy of combined tPA-edaravone therapy in experimental thrombotic stroke. *PLoS One*. 2014; 9:e98807. [PubMed: 24911517]
- Tondera D, Grandemange S, Jourdain A, Karbowski M, Mattenberger Y, Herzig S, Da Cruz S, Clerc P, Raschke I, Merkwirth C, Ehses S, Krause F, Chan DC, Alexander C, Bauer C, Youle R, Langer T, Martinou JC. SLP2 is required for stress-induced mitochondrial hyperfusion. *EMBO J*. 2009; 28:1589–1600. [PubMed: 19360003]
- Torii M, Hashimoto-Torii K, Levitt P, Rakic P. Integration of neuronal clones in the radial cortical columns by EphA and ephrin-A signalling. *Nature*. 2009; 461:524–528. [PubMed: 19759535]
- Zimmer A, Zimmer AM, Hohmann AG, Herkenham M, Bonner TI. Increased mortality, hypoactivity, and hypoalgesia in cannabinoid CB₁ receptor knockout mice. *Proc Natl Acad Sci USA*. 1999; 96:5780–5785. [PubMed: 10318961]
- Vanlangenakker N, Vanden Berghe T, Vandenabeele P. Many stimuli pull the necrotic trigger, an overview. *Cell Death Differ*. 2012; 19:75–86. [PubMed: 22075985]

Abbreviations

3D	three-dimensional
CB₁	cannabinoid type 1 receptor
E	embryonic day
L15	last 15 amino acids
L31	last 31 amino acids
LGE	lateral ganglionic eminence
DAB-Ni	Ni-intensified 3,3'-diaminobenzidine-4HCl
SLP2	stomatin-like protein 2
SVZ	subventricular zone
VZ	ventricular zone

**Fig. 1.**

Repetitive anti-CB₁-L31 (made-in-Guinea pig) and anti-SLP2 Western blots of the same membrane. Each column displays crudely purified mitochondrial preparation from one embryo or newborn mouse of the indicated age. (A) Anti-CB₁ labeling immediately after electrophoresis (left plate) shows weak, if any, staining; whereas 5 days later (right plate), anti-CB₁ labeling was markedly increased (Note the photo-exposure was reduced from 7 min to 30 sec). The ~60 kDa CB₁-band represents contamination of CB₁-containing membrane fragments from synaptosomes (Morozov *et al.*, 2013). (B) Anti-SLP2 antibody intensely labels ~40 and ~35 kDa SLP2 molecules in 2 days after electrophoresis (left plate), but the immuno-reactivity was greatly decreased after re-probing the membrane 5 days later (right plate). Photo-exposure was equal (8 sec) in both probes.

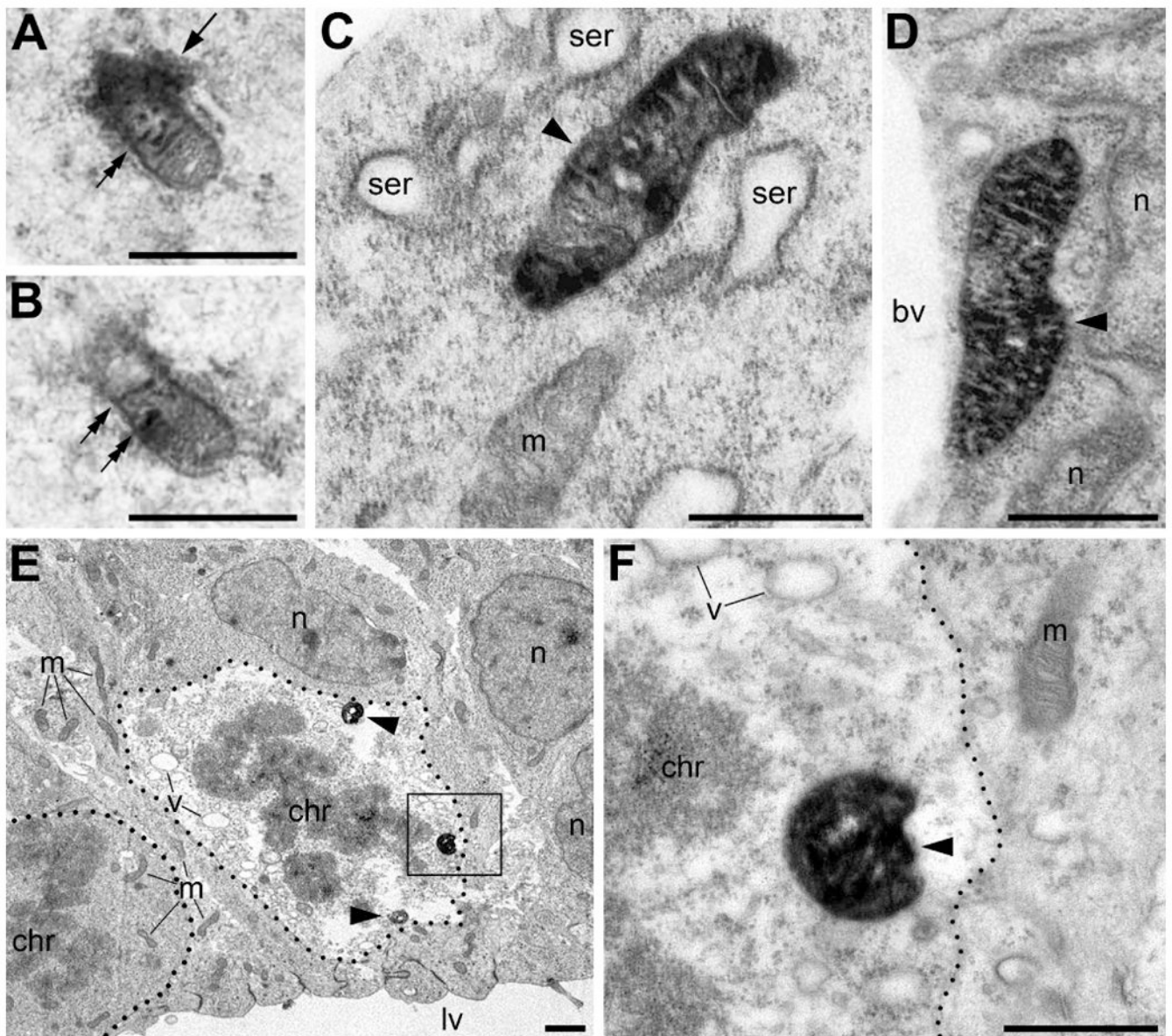


Fig. 2. Anti-CB₁-L31 made-in-Guinea pig antibody detected two types of immunopositive mitochondria in the neocortex of E13.5 mouse embryos: type 1 (A, B) and type 2 mitochondria (C-F). (A, B) Serial micrographs of a type 1 mitochondrion in the marginal zone. Notice characteristic immunoprecipitation in the cristae (double arrows) and around the mitochondrion (arrow). (C, D) Type 2 mitochondria (arrowheads) in an immature projection neuron (C) and an endothelial cell (D). Notice robust staining in the mitochondrial matrix whereas cristae are immunonegative. (E, F) Two mitotic metaphase cells (outlined with the dotted lines) in the ventricular zone facing the lateral ventricle (lv). The cell in the left lower corner of E contains only immunonegative mitochondria (m) and no detectable ultrastructural pathologies. In contrast, the adjacent mitotic cell (in the center of E) contains multiple type 2 mitochondria (arrowheads) and evidences for degradation, as

shown by numerous empty vacuoles (v) and diminished electron density in the cytoplasm. The framed area in E is enlarged in F. Scale bars: 1 μm (E); 0.5 μm (A-D, F). bv, lumen of blood vessel; chr, chromosomes in mitotic cells; n, cell nucleus; ser, swollen cisterns of rough endoplasmic reticulum.

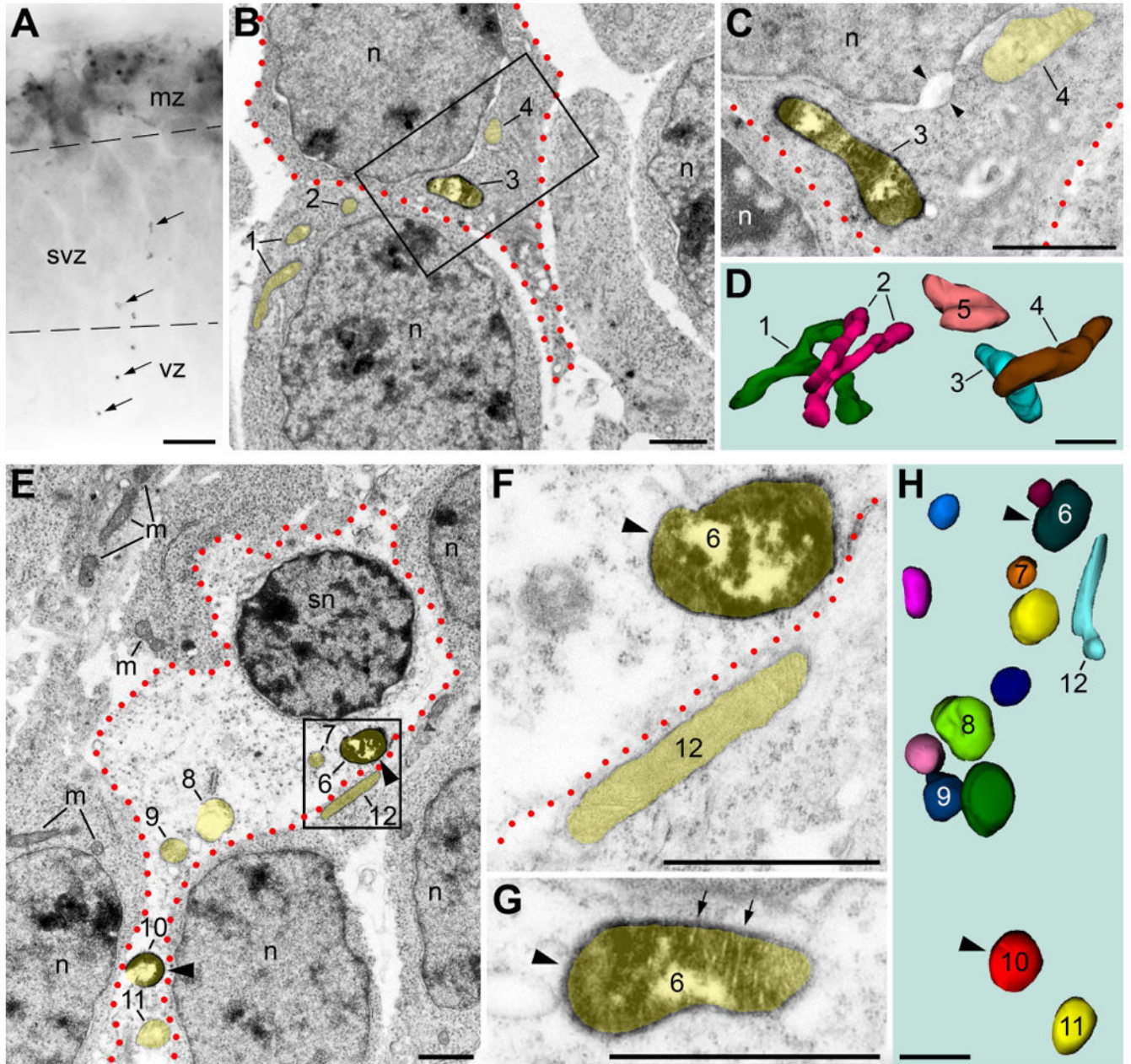


Fig. 3. Immunopositive mitochondria-containing neurons detected with anti-CB₁-L31 made-in-Guinea pig serum show both minor (A-D) and major (E-H) ultrastructural pathology in E12.5 mouse embryos. (A) Light microscopy reveals robust CB₁ immunolabeling in the marginal zone (mz) that is normal for the developing interneurons (Morozov *et al.*, 2009), as well as a subset of immunopositive mitochondria (arrows) in the ventricular zone (vz) and subventricular zone (svz). (B-D) Electron microscopy with 3D reconstruction from the tissue segment displayed in A demonstrates an immunopositive mitochondria-containing neuron (outlined with red dotted line) with minor ultrastructural pathology such as enlarged nuclear membrane (coupled arrowheads in C). Mitochondrial profiles are highlighted with

semitransparent yellow and respectively numbered in the electron micrographs and corresponding 3D images. Both, immunopositive (e.g., # 3) and immunonegative mitochondria (e.g., # 4 and 5) of this neuron are slightly swollen. Thin branched mitochondria #1 and #2 exemplify normal mitochondria of immunonegative neurons. The framed area in (B) is shown in (C) as a high power micrograph taken from a serial section. (E-H) A neocortical SVZ neuron (outlined with red dotted line) with major ultrastructural pathology (such as sphere-shaped nucleus [sn] and near-translucent cytoplasm) contains multiple swollen, sphere-shaped mitochondria that could be either immunopositive (arrowheads, #6 [shown with magnified serial images in F and G] and 10) or immunonegative (#7, 8, 9, and 11). In contrast, the surrounding immunonegative neurons contain morphologically normal mitochondria (m; e.g., #12), ovoid nuclei (n), and normal cytoplasm characteristic of developing neurons. Scale bars: 10 μm (A); 1 μm (B-H).

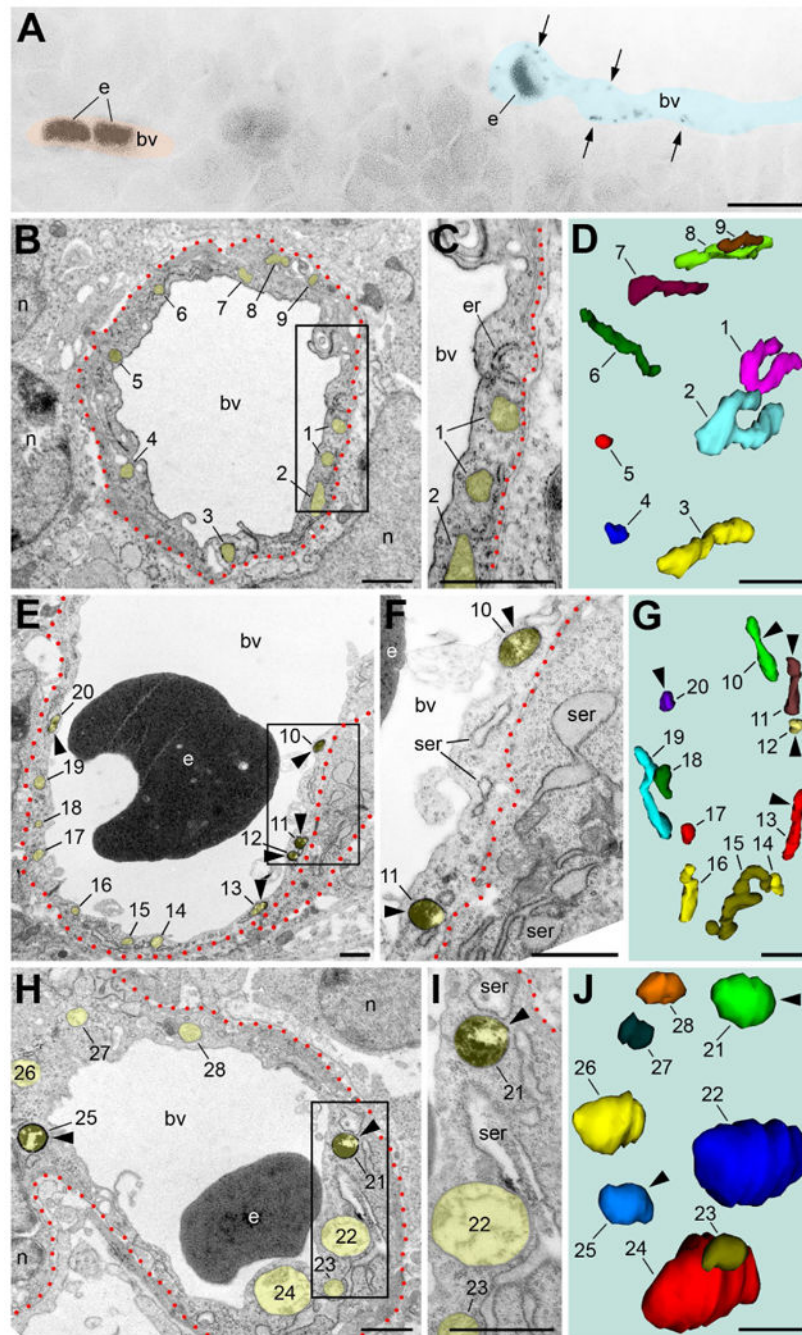


Fig. 4. Immunolabeling with CB₁-L31 made-in-Guinea pig serum distinguishes between normal (B-D) and pathological (E-J) endothelial cells in the subventricular zone of mouse embryos. (A) Light micrograph shows multiple immunopositive mitochondria (arrows) in a segment of blood vessel (bv; highlighted with semitransparent blue) while the neighboring segment (highlighted with semitransparent red) is immunonegative. (B-D) An immunonegative endothelial cell (outlined with red dotted line) contains thin elongated mitochondria and other organelles in normal cytoplasm. (E-J) In contrast, immunopositive mitochondria-

containing endothelial cells demonstrate minor (E-G) or major ultrastructural pathology (H-J), such as swollen mitochondria and cisterns of rough endoplasmic reticulum (ser). The framed areas in B, E and H are enlarged in C, F and I, respectively. D, G, and J show 3D reconstruction of the numbered mitochondria in B, E and H, respectively. Scale bars: 10 μm (A); 1 μm (B-J). e, erythrocyte; er, rough endoplasmic reticulum; n, cell nucleus.

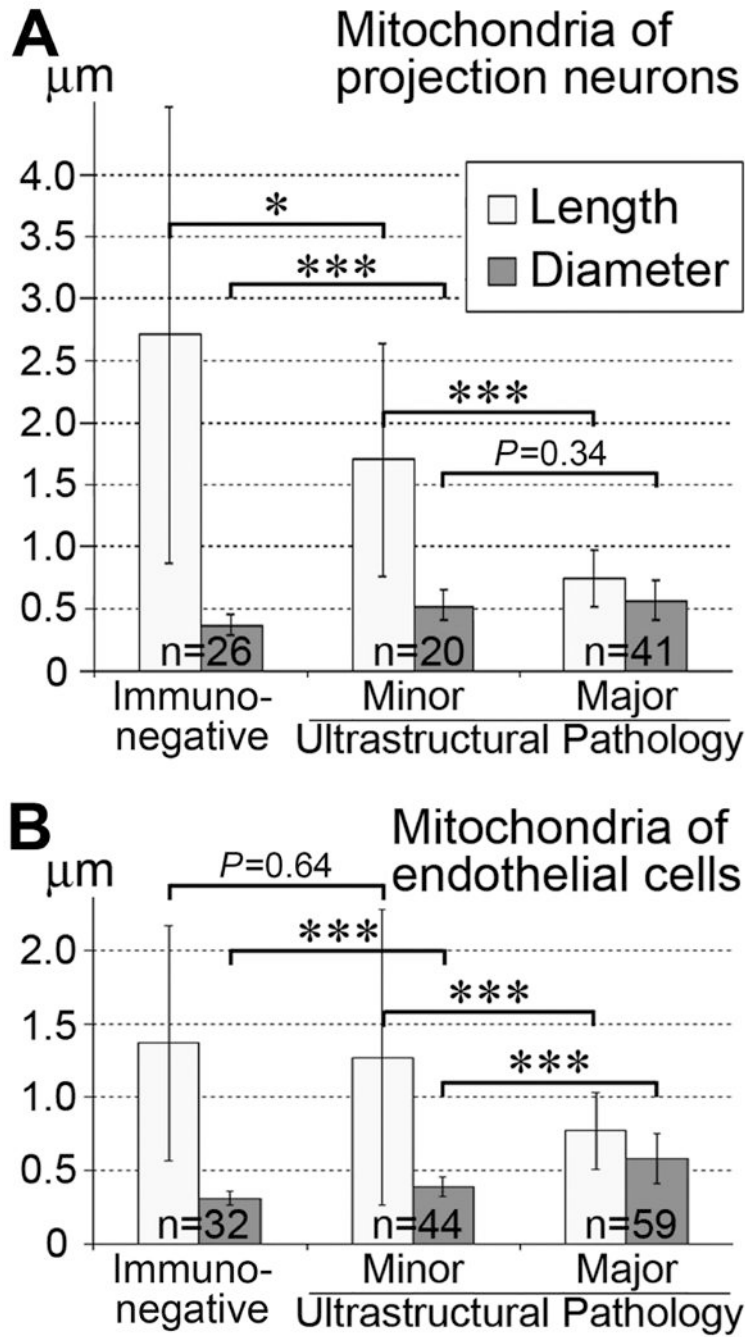


Fig. 5. Morphometric comparison of immunonegative and immunopositive (detected with CB₁-L31 made-in-Guinea pig serum) mitochondria in the developing projection neurons (A) and endothelial cells (B) in the mouse embryonic neocortex. The columns “Minor” and “Major Ultrastructural Pathology” characterize a varying degree of ultrastructural pathology for cells containing immunopositive mitochondria (more details in Table 1). The Y-axis shows the average length and diameter of mitochondria ± SD. Notice that the length of

mitochondria gradually decreases and their diameter increases as ultrastructural pathology become more apparent in both cell types. * $P < 0.05$; *** $P < 0.001$

Author Manuscript

Author Manuscript

Author Manuscript

Author Manuscript

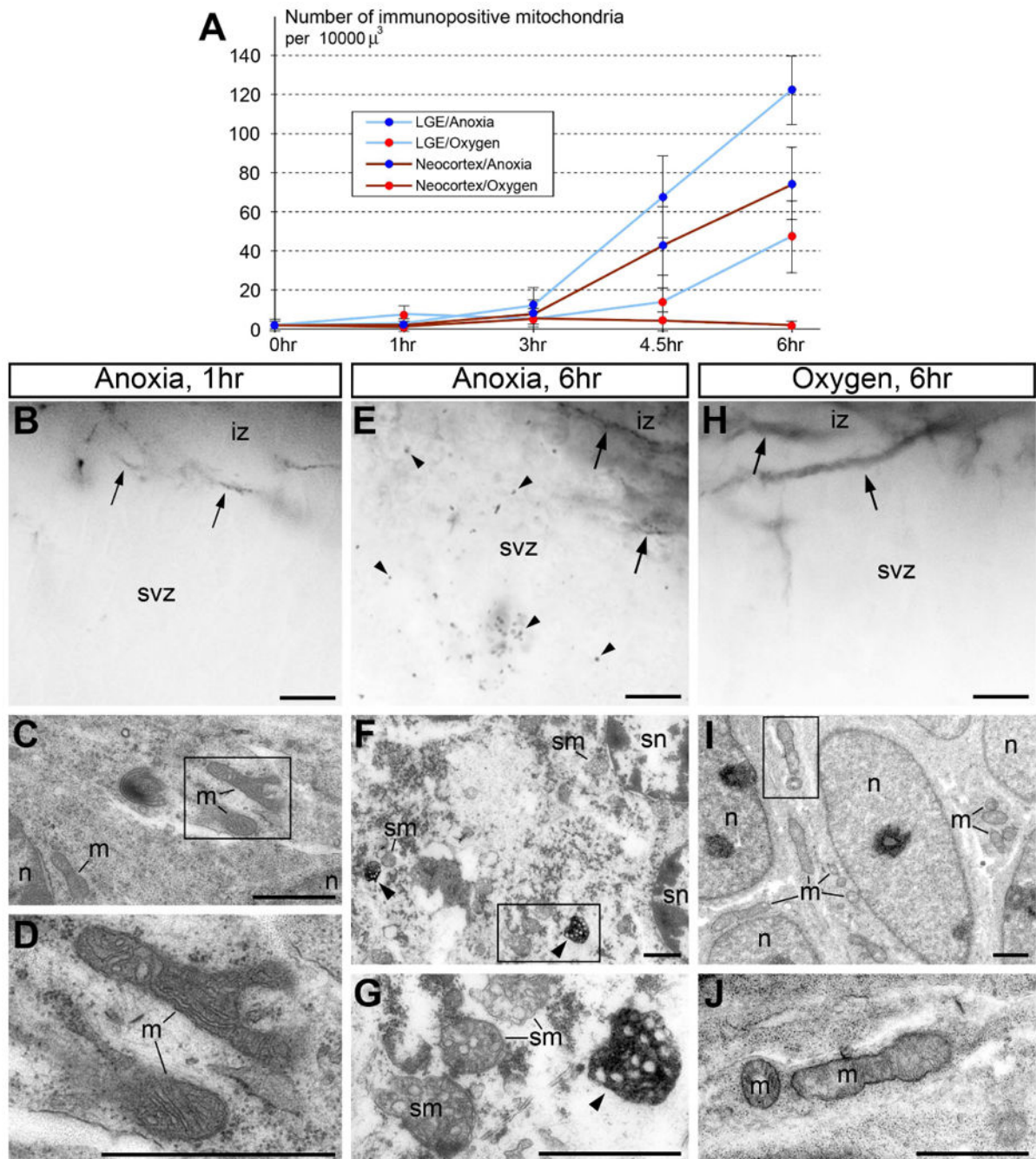


Fig. 6. Oxygenation of postmortem E13.5 mouse embryonic brains attenuates the rise of immunopositive mitochondria (detected with CB₁-L31 made-in-Guinea pig serum) and necrosis-like ultrastructural pathology. (A) Quantification of immunopositive mitochondria in the subventricular zone (svz) of postmortem brains in anoxia conditions or with oxygenation. Shown are the average \pm SD. (B-J) Representative light (B, E and H) and electron micrographs (C, D, F, G, I, and J) of anti-CB₁ labeling of the neocortical SVZ and intermediate zone (iz) that contain normal CB₁-positive axons (arrows in B, E and H) under

the indicated conditions. (B-D) At 1 hr anoxia, postmortem neurons retain normal structure of nuclei (n) and organelles including mitochondria (m) that are negative for anti-CB₁-L31 labeling. (E-G) At 6 hr anoxia, postmortem neurons show numerous immunopositive mitochondria (arrowheads) and necrosis-like ultrastructural pathologies, such as spherical-shape nuclei (sn) and swollen mitochondria (sm). (H-J) In contrast, dissected embryonic brains immersed in the oxygenated medium demonstrate very few, if any, immunopositive mitochondria (H) and mostly normal ultrastructure in postmortem neurons (I and J). Framed areas in C, F and I are enlarged in D, G and J, respectively. Scale bars: 10 μm (B, E and H); 1 μm (C, D, F, G, I, and J). m, mitochondria; n, nucleus; svz, subventricular zone.

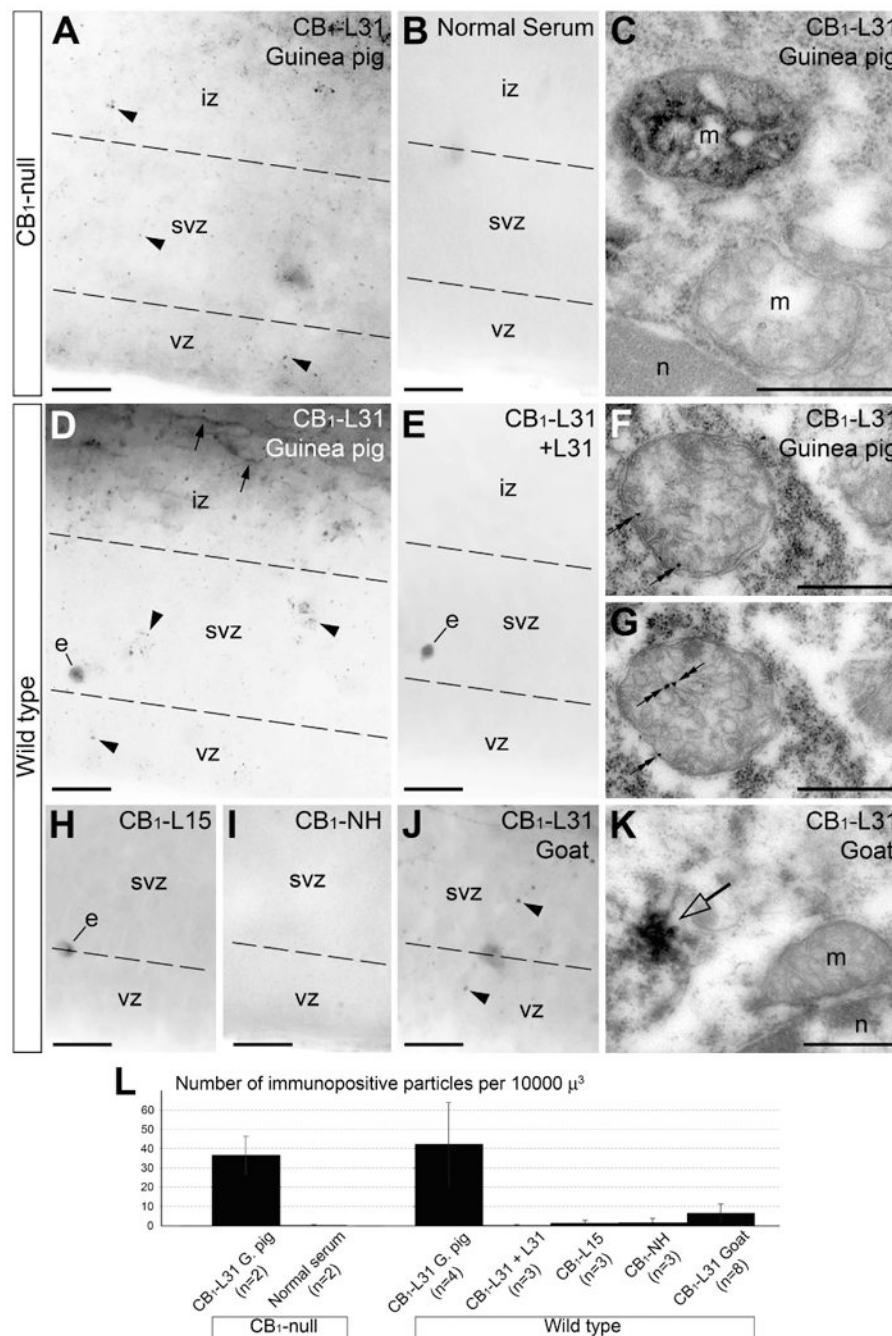


Fig. 7. Immunolabeling of E13.5 embryos after 4.5 hr postmortem anoxia with different anti-CB₁ sera in CB₁-null and wild-type mice. (A-C) In CB₁-null embryos, canonical CB₁ labeling is absent whereas staining of mitochondria with CB₁-L31 made-in-Guinea pig serum and DAB-Ni as a chromogen (arrowheads) is robust (A). Replacing the primary antibody with normal Guinea pig serum abolishes mitochondrial labeling (B). Electron microscopy confirms abundance of immunopositive mitochondria (m; upper one) in the CB₁-null embryos; immunonegative mitochondria are also seen (C). (D, E) In a wild type littermate,

anti-CB₁-L31 made-in-Guinea pig serum with DAB-Ni as a chromogen produces mitochondrial (arrowheads) and canonic axonal CB₁ labeling (arrows; D) whereas pre-absorption of the serum with the L31 peptide blocks both types of staining (E). (F, G) Immunolabeling with nano-gold/silver as a chromogen (double arrows) shows matrix location of the antigen in serial micrographs of a mitochondrion. (H, I) Sera raised to L15 and NH segments of CB₁ do not provide labeling of mitochondria with DAB-Ni as a chromogen. (J, K) Anti-CB₁-L31 serum made-in-goat produces dotted staining (arrowheads) that looks similar to mitochondrial labeling in light microscope (J) nevertheless electron microscopy reveals cytoplasmic staining whereas mitochondrial labeling was not encountered in these specimens (K). (L) Quantification of immunopositive mitochondria identified in light microscope as stained particles in the subventricular zone (svz) of postmortem brains using different primary sera and DAB-Ni as a chromogen in wild type and CB₁-null embryos. Shown are the average \pm SD. n is the number of embryos analyzed. Notice the high level of labeling in wild type and CB₁-null with CB₁-L31 made-in-Guinea pig serum whereas the serum pre-absorbed with L31 peptide and other sera produce little if any labeling. The dashed lines delineate the borders between ventricular (vz), subventricular (svz) and intermediate zones (iz). Scale bars: 20 μ m (A, B, D, E, H-J); 0.5 μ m (C, F, G, K). e, erythrocyte; n, cell nucleus.

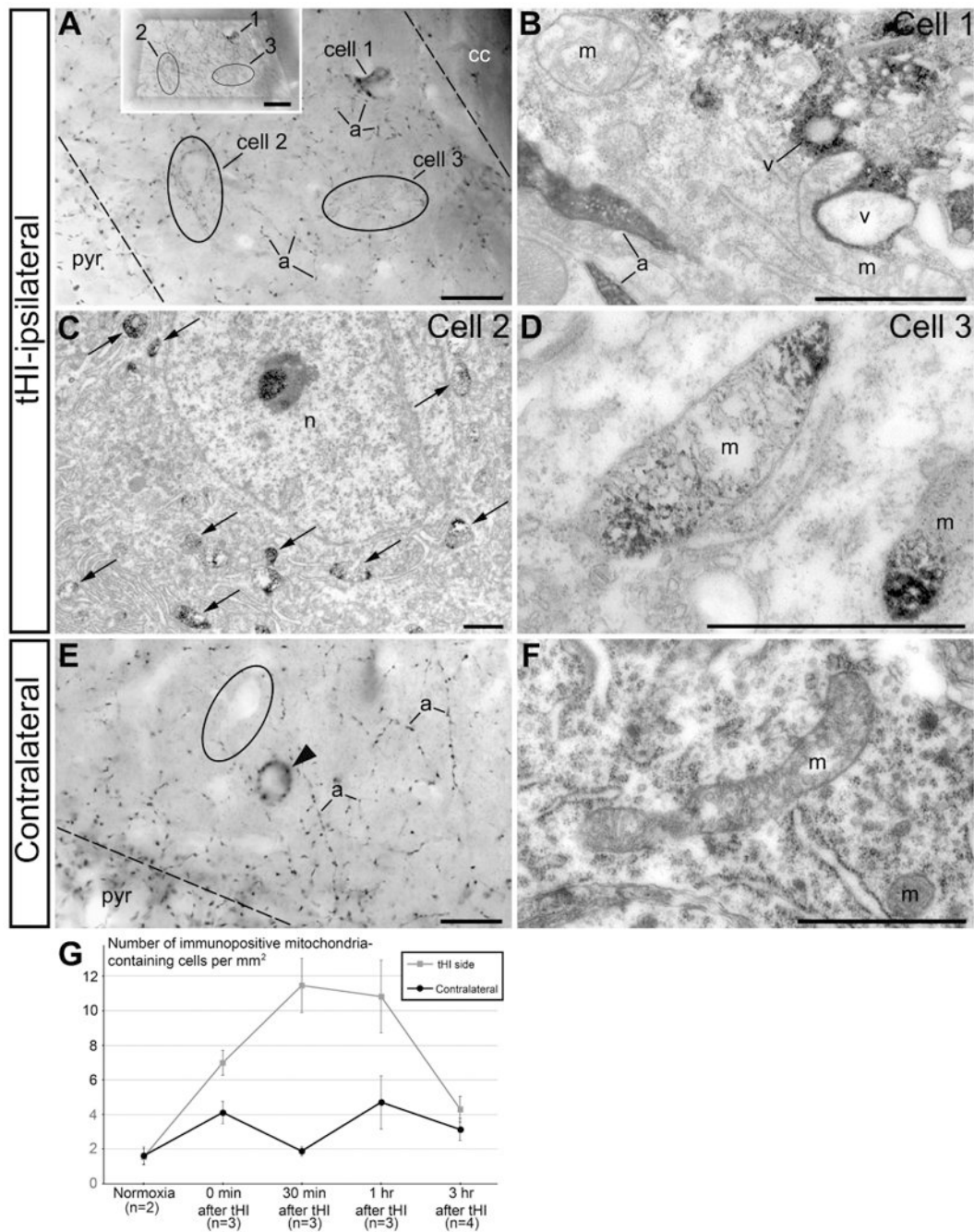


Fig. 8. Anti-CB₁-L31 (made-in-Guinea pig) immunolabeling in the hippocampal CA1 orients on the tHI-exposed hemisphere (A-D) and contralateral side (E, F) in 30 min after tHI. (A) Light micrograph of 3 immunopositive cells, of which cell 1 contains robust somatic CB₁ staining, while cell 2 and 3 (indicated with ovoid) show punctate staining in the cell body and proximal dendrites. Borders of the stratum oriens are indicated with dashed lines. Insertion shows the specimen that is trimmed for ultrathin sectioning and correlative light/electron microscopy examination of these numbered cells. (B) Electron micrograph shows that cell 1

contains immunonegative mitochondria, and its robust staining is due of somatic CB₁ located on the outer surface of intracellular vesicles (v) that are characteristic for CB₁-expressing interneurons. CB₁-immunopositive axons (a) are also seen in the light and electron micrographs. (C, D) In contrast, cells 2 and 3 contain numerous immunopositive mitochondria (arrows in C). (D) High-power electron micrograph of typical swollen mitochondria from cell 3 shows that immunoreaction end-product concentrates in the mitochondrial matrix, while the cristae are immunonegative. (E) Light micrograph of hippocampal stratum oriens from the contralateral side show numerous CB₁-positive axons (a), a CB₁-positive cell body (arrowhead), and an adjacent immunonegative cell (ovoid). (F) Representative mitochondria (m) from a hippocampal interneuron in the contralateral side. Notice the absence of swelling in the immunonegative mitochondria. (G) Quantification of immunopositive mitochondria-containing cells (normalized per 1 mm²) in the hippocampus in the tHI-exposed and contralateral sides. Scale bars: 20 μm (A, insertion and E); 1 μm (B-D and F). n, cell nucleus; cc, corpus callosum; pyr, pyramidal cell layer.

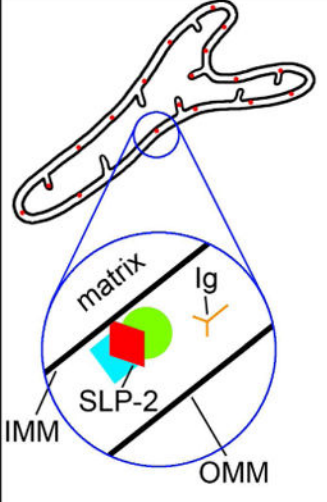
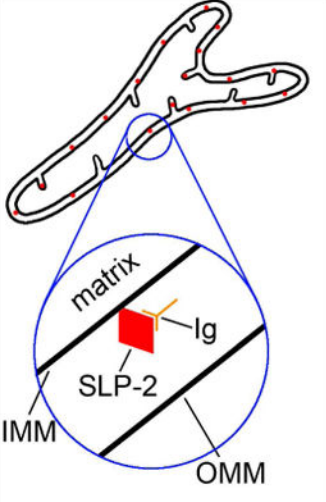
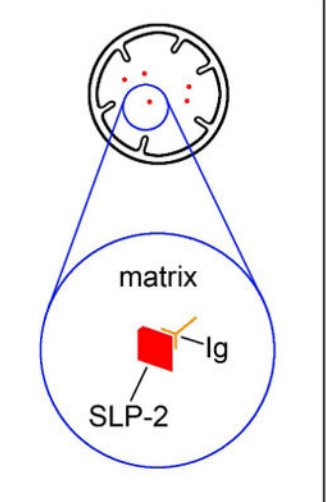
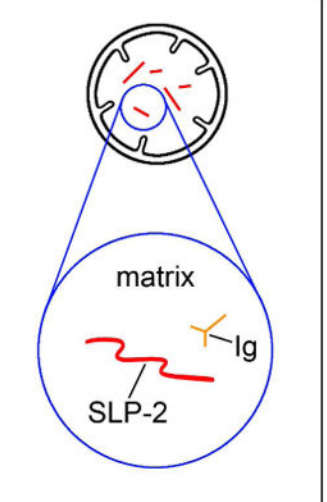
Immunonegative Normal shape	Immunopositive Type 1	Immunopositive Type 2	Immunonegative Swollen
 <p>The diagram shows a normal mitochondrion with a tubular shape. A circular inset provides a magnified view of the inner mitochondrial membrane (IMM) and outer mitochondrial membrane (OMM). The IMM is shown as a red cube-like structure with a green circle (SLP-2) attached to its surface. An antibody (Ig) is shown as a yellow Y-shape. The matrix is the space between the membranes, and the intermembrane space is the space between the IMM and OMM. Other molecules are shown blocking the epitope.</p>	 <p>The diagram shows a mitochondrion with a tubular shape. A circular inset provides a magnified view of the IMM and OMM. The SLP-2 (red cube) is attached to the IMM, and the antibody (Ig, yellow Y-shape) is bound to it. The matrix and intermembrane space are also labeled.</p>	 <p>The diagram shows a mitochondrion with a tubular shape. A circular inset provides a magnified view of the matrix. The SLP-2 (red cube) is located in the matrix, and the antibody (Ig, yellow Y-shape) is bound to it. The IMM and OMM are also labeled.</p>	 <p>The diagram shows a swollen mitochondrion with a circular shape. A circular inset provides a magnified view of the matrix. The SLP-2 (red cube) is denatured and shown as a red wavy line. The antibody (Ig, yellow Y-shape) is bound to it. The matrix and intermembrane space are also labeled.</p>
<p>SLP-2 in normal tertiary structure is attached to the IMM facing the intermembrane space. Other molecules block the epitope.</p>	<p>SLP-2 maintains normal tertiary structure. Reorganization of protein supercomplexes releases the epitope for immunolabeling.</p>	<p>SLP-2 in normal tertiary structure is relocated in the mitochondrial matrix. The epitope is available for immunolabeling.</p>	<p>SLP-2 is denaturalized. The epitope is destroyed.</p>

Fig. 9. Hypothetic schema of the relationships between mitochondrial morphology, molecular conformation/location of the SLP2 protein and CB₁-L31 antibody (Ig). IMM, inner mitochondrial membrane; OMM, outer mitochondrial membrane.

Table 1
Morphometric characterization of mitochondria in certain cell types of the mouse embryo neocortex

Mitochondrial type	Number of mitochondria analyzed	Volume, $\mu\text{m}^3 \pm \text{SD}$	Estimated length, μm			Mean diameter, $\mu\text{m} \pm \text{SD}$	Length / Diameter $\pm \text{SD}$
			Average $\pm \text{SD}$	Min	Max		
1. Horizontal neurons in MZ (Presumed migrating interneurons; E13.5)							
Immunonegative	88	0.07±0.06	1.3±1.1	0.3	6.4	0.33±0.05	4.1±3.8
Type 1	14	0.07±0.05	1.5±1.0	0.6	3.9	0.30±0.05	5.2±3.3
Type 2	Not found	-	-	-	-	-	-
2. Projection neurons							
2.1. Vertical neurons in VZ/SVZ (E12.5)							
Immunonegative	26	0.20±0.20	2.7±1.8	0.6	6.9	0.37±0.08	7.7±5.8
Type 1	Not found	-	-	-	-	-	-
Type 2	Not found	-	-	-	-	-	-
2.2. Neurons with minor ultrastructural pathologies in VZ/SVZ (E12.5) *							
Immunonegative	15	0.23±0.13	1.8±1.0	0.5	3.5	0.51±0.12	3.7±2.3
Type 1	Not found	-	-	-	-	-	-
Type 2	5	0.28±0.11	1.6±0.9	0.7	2.9	0.60±0.11	2.8±1.9
2.3. Neurons with major ultrastructural pathologies in VZ/SVZ (E13.5) **							
Immunonegative	27	0.12±0.08	0.7±0.2	0.4	1.0	0.52±0.13	1.3±0.3
Type 1	Not found	-	-	-	-	-	-
Type 2	14	0.25±0.17	0.9±0.2	0.5	1.3	0.67±0.17	1.4±0.3
3. Endothelial cells							
3.1. Normal endothelial cells (E17.5)							
Immunonegative	32	0.07±0.06	1.4±0.8	0.4	3.0	0.31±0.05	4.5±2.9
Type 1	Not found	-	-	-	-	-	-
Type 2	Not found	-	-	-	-	-	-
3.2. Endothelial cells with minor ultrastructural pathologies (E13.5) *							
Immunonegative	30	0.08±0.06	1.2±1.0	0.3	4.3	0.37±0.05	3.4±3.0
Type 1	Not found	-	-	-	-	-	-

Mitochondrial type	Number of mitochondria analyzed	Volume, $\mu\text{m}^3 \pm \text{SD}$	Estimated length, μm			Mean diameter, $\mu\text{m} \pm \text{SD}$	Length / Diameter $\pm \text{SD}$
			Average $\pm \text{SD}$	Min	Max		
Type 2	13	0.12 \pm 0.07	1.4 \pm 1.1	0.4	4.3	0.42 \pm 0.09	3.6 \pm 3.2
3.3. Endothelial cells with major ultrastructural pathologies (E17.5) **							
Immunonegative	38	0.16 \pm 0.15	0.7 \pm 0.2	0.4	1.3	0.58 \pm 0.16	1.3 \pm 0.2
Type 1	Not found	-	-	-	-	-	-
Type 2	21	0.20 \pm 0.22	0.8 \pm 0.3	0.4	1.5	0.59 \pm 0.20	1.4 \pm 0.3

* The cells contain type 2 mitochondria and demonstrate minor ultrastructural pathologies such as swollen cisterns of rough endoplasmic reticulum and/or swollen nuclear membrane (exemplified in Fig. 3B-D and Fig. 4E-G).

** The cells contain type 2 mitochondria and demonstrate considerable vacuolization and degradation of cytoplasm (exemplified in Fig. 3E-H and Fig. 4H-J).

Table 2
Density* of immunopositive mitochondria in VZ/SVZ mouse embryo neuropil upon exposure to anoxia or oxygenation for different lengths of time at +37°C

	0hr		1hr		3hr		4.5hr		6hr	
	n=6	Anoxian=4	Oxygen n=2	Anoxia n=6	Oxygen n=2	Anoxia n=4	Oxygen n=4	Anoxia n=2	Oxygen n=2	Anoxia n=2
LGE	1.9±2.3	2.8±2.8	7.2±5.3	11.9±9.2	5.0±3.8	67.5±21.6	13.9±13.9	122.4±17.6	47.5±18.2	
Neo-cortex	2.3±3.1	1.0±1.2	1.5±2.3	7.6±7.1	5.5±5.6	42.4±21.5	4.0±5.0	73.7±19.4	2.1±1.9	
Dorsal arch	5.6±6.5	1.4±1.8	0.9±1.3	15.7±16.1	7.2±6.7	66.7±27.6	7.8±8.2	87.9±24.8	1.7±1.9	
Hippo-campus	7.3±10.5	1.3±1.4	0.6±0.9	13.1±11.4	3.6±4.0	69.0±20.9	2.9±2.6	92.1±18.9	6.3±8.1	

* Average numbers of immunopositive mitochondria per 10000 μm^3 of the neuropil obtained from 20 measurements from each embryo and brain segment \pm SD.
n is number of analyzed embryos.